JACC: CARDIOVASCULAR IMAGING VOL. 4, NO. 10, 2011

ISSN 1936-878X/$36.00
PUBLISHED BY ELSEVIER INC. DOI:10.1016/j.jcmg.2011.04.020

Pioglitazone Modulates Vascular Inflammation in Atherosclerotic Rabbits

Noninvasive Assessment With FDG-PET-CT and Dynamic Contrast-Enhanced MR Imaging

Esad Vucic, MD,*† Stephen D. Dickson, MS,* Claudia Calcagno, MD, PhD,*‡ James H. F. Rudd, MD, PhD,§ Erin Moshier, MS,‖ Katsumi Hayashi, MD,* Jessica S. Mounessa, BS,* Michelle Roytman, BS,* Matthew J. Moon, BS,* James Lin, MS,* Sotirios Tsimikas, MD,¶ Edward A. Fisher, MD, PhD,# Klaas Nicolay, PhD,** Valentin Fuster, MD, PhD,† †† Zahi A. Fayad, PhD*†‡
New York, New York; Cambridge, United Kingdom; La Jolla, California; Eindhoven, the Netherlands; and Madrid, Spain

OBJECTIVES We sought to determine the antiatherosclerotic properties of pioglitazone using multimethod noninvasive imaging techniques.

BACKGROUND Inflammation is an essential component of vulnerable or high-risk atheromas. Pioglitazone, a peroxisome proliferator-activated receptor-gamma agonist, possesses potent anti-inflammatory properties. We aimed to quantify noninvasively the anti-inflammatory effects of pioglitazone on atheroma using ^{18}F-fluorodeoxyglucose (^{18}F-FDG) positron emission tomography (PET)/computed tomography (CT) and dynamic contrast-enhanced (DCE) magnetic resonance imaging (MRI).

METHODS Atherosclerotic plaques were induced in the aorta of 15 New Zealand white rabbits by a combination of a hyperlipidemic diet and 2 balloon endothelial denudations. Nine rabbits continued the same diet, whereas 6 rabbits received pioglitazone (10 mg/kg orally) in addition to the diet. Twelve animals underwent ^{18}F-FDG-PET/CT, and 15 animals underwent DCE-MRI at baseline, 1 month, and 3 months after treatment initiation. Concomitantly, serum metabolic parameters were monitored. After imaging was completed, aortic histologic analysis and correlation analysis were performed.

RESULTS The ^{18}F-FDG-PET/CT imaging detected an increase in average standardized uptake value in the control group ($p < 0.01$), indicating progressive inflammation, whereas stable standardized uptake values were observed in the treatment group, indicating no progression. The DCE-MRI analysis detected a significant decrease in the area under the curve for the pioglitazone group ($p < 0.01$). Immunohistologic examination of the aortas demonstrated a significant decrease in macrophage and oxidized phospholipid immunoreactivity in the pioglitazone group ($p = 0.04$ and $p = 0.01$, respectively) with respect to control animals, underlining the imaging results. Serum metabolic parameters showed no difference between groups. Strong positive correlations between standardized uptake value and macrophage density and between area under the curve and neovessels were detected ($r^2 = 0.86$ and $p < 0.0001$, and $r^2 = 0.66$ and $p = 0.004$, respectively).

CONCLUSIONS Both ^{18}F-FDG-PET/CT and DCE-MRI demonstrate noninvasively the anti-inflammatory effects of pioglitazone on atheroma. Both imaging methods seem suited to monitor inflammation in atherosclerosis. (J Am Coll Cardiol Img 2011;4:1100–9) © 2011 by the American College of Cardiology Foundation

Cardiovascular disease remains the major cause of morbidity and mortality worldwide (1), despite the widespread use of low-density lipoprotein cholesterol-lowering therapies. Inflammation, mainly promoted by oxidized lipids in the vessel wall, plays a critical role in all stages of atherosclerosis, but is crucial in plaque rupture and thrombosis, which causes most acute coronary

See page 1119

events (2,3). Vulnerable plaques are characterized by a relatively large lipid core, a thin fibrous cap, and an abundance of inflammatory cells (especially macrophages) accompanied by neovascularization (4). Currently, therapies targeting reversal cholesterol transport and inflammation, in particular recombinant high-density lipoprotein therapeutics and various nuclear receptor agonists, are being developed (5). However, their translation into clinical practice has been difficult because of the lack of clinical outcome studies and validated surrogate endpoints (6).

The peroxisome proliferator-activated receptor gamma (PPAR-γ) belongs to a nuclear receptor superfamily of ligand-dependent transcription factors. Different cells involved in the pathogenesis of atherosclerosis, such as endothelial cells, smooth muscle cells, T-lymphocytes, dendritic cells, and mainly macrophages, express PPAR-γ receptor (7,8). Synthetic PPAR-γ receptor ligands, thiazolidinediones, are used in clinical practice as oral antidiabetic agents. Besides their antidiabetic properties, thiazolidinediones have demonstrated in animal studies potent antiatherosclerotic effects by inhibiting the formation of atherosclerotic plaques (9,10). However, some thiazolidinediones may increase the risk of myocardial infarction (11). Pioglitazone, in contrast, in the large clinical secondary prevention PROspective pioglitAzone Clinical Trial In macroVascular Events trial (more than 5,000 subjects), demonstrated a significant reduction of all-cause mortality, myocardial infarction, and stroke in a diabetic patient population (12). Two subsequent large trials (CHICAGO [Carotid Intima-Media Thickness in Atherosclerosis Using Pioglitazone] and PERISCOPE [Pioglitazone Effect on Regression of Intravascular Sonographic Coronary Obstruction Prospective Evaluation]) showed decreased progression of carotid intima-media thickness (as assessed by surface and intravascular ultrasounds) after 18 months of treatment with pioglitazone. These 2 studies confirmed the significant vascular benefits of pioglitazone and highlighted the potential role of imaging in tracking the progression of disease or its regression on therapeutic intervention. However, the imaging techniques used in these studies do not give any information regarding changes in vascular inflammation induced by pioglitazone, which may help to identify responsive patients much before anatomical changes become apparent. Noninvasive imaging techniques targeted toward quantifying inflammation, macrophage content, and neovascularization of atherosclerotic vessels represent an attractive clinical tool. In an ideal scenario, such techniques would allow an accurate readout of vessel wall inflammation, delineating cardiovascular risk, guiding therapeutic decisions, and defining the role of novel treatments, and therefore may aid in risk stratification and may provide surrogate therapeutic endpoints (13). Recently, a study in mice showed that noninvasive optical molecular imaging techniques can detect changes in inflammation on pioglitazone treatment (14). However, the techniques used in these studies cannot be applied in a clinical setting because of the limited depth penetration possible with

ABBREVIATIONS AND ACRONYMS

AU = arbitrary unit

AUC = area under the curve

$AUC_{1\ min}$ = area under the curve quantified at 1 minute

$AUC_{2\ min}$ = area under the curve quantified at 2 minutes

CT = computed tomography

DCE = dynamic contrast-enhanced

FDG = fluorodeoxyglucose

MRI = magnetic resonance imaging

PET = positron emission tomography

PPAR-γ = peroxisome proliferator-activated receptor gamma

SUV = standard uptake value

SUV_{max} = maximal standard uptake value

SUV_{mean} = mean standard uptake value

From the *Translational and Molecular Imaging Institute, Imaging Science Laboratories, Mount Sinai School of Medicine, New York, New York; ‡Department of Radiology, Mount Sinai School of Medicine, New York, New York; §Division of Cardiovascular Medicine, University of Cambridge, Cambridge, United Kingdom; ‖Biostatistics Shared Research Facility, Department of Community and Preventive Medicine, Mount Sinai School of Medicine, New York, New York; ¶Vascular Medicine Program, University of California San Diego, La Jolla, California; #Department of Cardiology, New York University School of Medicine, New York, New York; **Biomedical NMR, Department of Biomedical Engineering, Eindhoven University of Technology, Eindhoven, the Netherlands; ††The Zena and Michael A. Wiener Cardiovascular Institute and Marie-Josée and Henry R. Kravis Cardiovascular Health Center, Mount Sinai Hospital, New York, New York; and the ††Centro Nacional de Investigaciones Cardiovasculares (CNIC), Madrid, Spain. This investigation was supported in part by an investigator-initiated grant from Takeda Pharmaceutical (to Dr. Vucic); the Fondation Leducq (to Dr. Tsimikas); grants R01 HL071021 and R01 HL078667 from the National Heart, Lung and Blood Institute, National Institutes of Health (to Dr. Fayad); and grant EB009638 from the NBIB (National Institute of Biomedical Imaging and Bioengineering), National Institutes of Health (to Dr. Fayad). Dr. Tsimikas holds patents on oxidation-specific antibodies through the University of California San Diego. All other authors have reported that they have no relationships relevant to the contents of this paper to disclose. Mr. Dickson and Dr. Calcagno contributed equally to this work. H. William Strauss, MD, served as Guest Editor for this article.

Manuscript received March 4, 2011; revised manuscript received April 22, 2011, accepted April 22, 2011.

optical imaging. ^{18}F-fluorodeoxyglucose (^{18}F-FDG) positron emission tomography (PET)/computed tomography (CT) and dynamic contrast-enhanced (DCE) magnetic resonance imaging (MRI) are noninvasive, clinically available techniques and recently have been validated as indicators of vascular inflammation: ^{18}F-FDG-PET/CT detected vascular macrophage content and DCE-MRI detected neovascularization (15–18). In this study, we applied ^{18}F-FDG-PET/CT and DCE-MRI to characterize vascular inflammation and neovascularization and its changes during pioglitazone treatment in a rabbit model of atherosclerosis.

METHODS

Animal model. Fifteen New Zealand white rabbits (Charles River Laboratories, Inc., Wilmington, Massachusetts) at the age of 3 months (weight: 3.0 ± 0.1 kg) were fed a diet containing 0.3% cholesterol and 4.7% coconut oil for 3 months and 0.15% cholesterol and 4.7% coconut oil thereafter. The development of atherosclerosis was enhanced further with a double balloon injury to the abdominal aorta at weeks 2 and 6 (19). At 4 months, the animals were divided into 2 groups (control: n = 9, treatment: n = 6). The treatment group received pioglitazone (10 mg/kg body weight) (20) mixed with the high-fat diet for 3 months (Fig. 1). Three age-matched animals on a chow diet served as nonatherosclerotic controls. Diets were prepared by Research Diets Inc. (New Brunswick, New Jersey). All procedures were performed under anesthesia by intramuscular injection of ketamine (20 mg/kg) (Fort Dodge Animal Health, Overland Park, Kansas) and xylazine (5 mg/kg) (Bayer AG, Leverkusen, Germany). The protocol was approved by the Mount Sinai School of Medicine Institute Animal Care and Use Committee.

Serum analysis and fast protein liquid chromatography. Blood was collected from 12-h fasting animals at baseline, 4, 5, and 7 months after high-cholesterol diet and was separated into serum per standard protocols (21). Serum samples were analyzed using commercial kits for cholesterol, triglycerides, glucose, and insulin. In addition, pooled serum at baseline and after 3 months of pioglitazone treatment was subjected to fast protein liquid chromatography.

Immunohistologic analysis. Macrophages were detected on adjacent slices by standard immunohistochemistry techniques. The total macrophage-rich (RAM-11–positive) area was quantified digitally as fraction of the intimal-media area (i.e., macrophage density) per slice and was expressed as the average macrophage density per animal. Similarly, the areas for smooth muscle actin, apolipoprotein B-100, and oxidized phospholipids were evaluated. Neovessels were

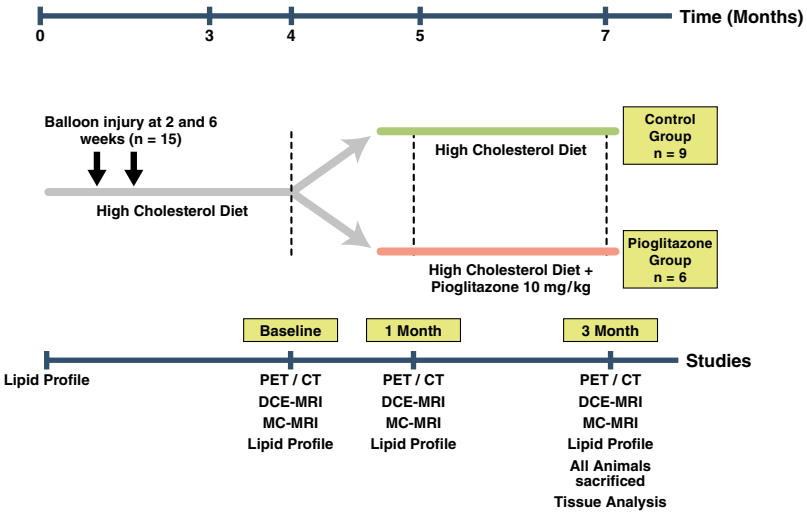

Figure 1. Study Design

Atherosclerosis was induced in 15 New Zealand white rabbits through a combination of double-balloon injury and high cholesterol diet. After 4 months of the diet, the first imaging scans and lipid profiles were performed (baseline), and animals were divided into 2 groups: a control group and a pioglitazone group. After a total of 5 months, another round of imaging scans and lipid profiles (1-month imaging) were performed. The final imaging scans and lipid profiles were performed after a total of 7 months (3-month imaging). All animals then were killed immediately and tissue analysis was performed. DCE-MRI = dynamic contrast-enhanced magnetic resonance imaging; MC-MRI = multicontrast-magnetic resonance imaging; PET/CT = positron emission tomography/computed tomography.

detected on a single DCE image matched section with an anti-CD31 antibody, as previously described (17).

^{18}F-FDG-PET/CT. Six rabbits from each group were imaged using a combined PET/CT scanner (Discovery LS, GE Healthcare). The PET images were acquired for 10 min, 3 h after intravenous injection of ^{18}F-FDG (37 MBq [1 mCi/kg]) (19). The images were acquired in 3-dimensional mode, and the acquisition covered the area from the diaphragm to the iliac bifurcation. A Fourier iterative reconstruction of the PET data was used. In addition to a PET scan, a non–contrast-enhanced CT scan was obtained for each rabbit on the same scanner for attenuation correction and anatomical localization of the PET signal. The final reconstructed slice thickness was 4.25 mm.

PET/CT analysis. The PET/CT data were displayed in 3 orthogonal planes on a GE Xeleris workstation. Maximal standard uptake values (SUV_{max}) and mean standard uptake values (SUV_{mean}) were recorded on contiguous axial slices of the aorta between the left renal artery and the iliac bifurcation (average number of slices: 13.6) from regions of interest encompassing the vessel wall. Results were expressed as the average SUV_{mean} of the aorta per animal.

Anatomic and DCE-MRI. Nine control and 6 pioglitazone-treated rabbits were imaged under anesthesia using a 1.5-T MRI system (Siemens Sonata, Siemens Medical Solutions) and a conventional knee coil. Sequential axial, 3-mm thick images of the aorta were obtained from the left renal artery to the iliac bifurcation using T1-weighted, T2-weighted, and PD (proton density)-weighted imaging sequences. The DCE-MRI was performed on 1 selected axial slice using a black blood turbo spin echo sequence previously validated against histologic analysis (17).

Anatomic multicontrast-MRI and DCE-MRI analysis. Average vessel wall area of the aorta between the left renal artery and iliac bifurcation was quantified on contiguous slices by manual tracing on T2-weighted images (VesselMass Software, Leiden University Medical Center). Then, DCE-MRI quantified the change of signal intensity in a region of interest including the entire atherosclerotic plaque during the injection of the contrast agent with a custom-made Matlab (The MathWorks Inc., Natick, Massachusetts) program. The area under the curve (AUC) was quantified at 1 min (AUC_{1min}) and at 2 min (AUC_{2min}) after injection of contrast agent by numerical integration (17).

Statistical analysis. Numeric values are expressed as mean ± SD. A p value <0.05 was considered statistically significant. Continuous DCE-MRI and PET outcomes were modeled as linear functions of time for both treatment and control groups. A linear mixed model with random intercepts and compound symmetric covariance structure was used to estimate the regression equations for treatment and control groups while accounting for the correlation between repeated measurements made on each rabbit (22). The models for PET outcomes were weighted by the number of slices analyzed in each animal. To test for differences among the treatment and control groups estimated by linear regression equations, an interaction term between treatment group and time was included in each mixed model along with both main effects. If the interaction term was found to be statistically significant, then pairwise comparisons of treatment group slopes were estimated. All statistical analyses were performed using Proc Mixed in SAS software version 9.2 (SAS Institute, Cary, North Carolina). Average macrophage density per animal was correlated with average animal SUV_{max} or AUC_{1min} of the corresponding animal. Neovessels were counted on a single section, were matched to the DCE-MRI imaged slice, and were correlated with AUC_{1min} or

Table 1. Animal Characteristics

	Control (n = 9)	PIO (n = 6)	p Value
Weight (kg)			
t = 4 months	3.42 ± 0.29	3.32 ± 0.33	0.52
t = 5 months	3.47 ± 0.31	3.29 ± 0.40	0.32
t = 7 months	3.42 ± 0.38	3.40 ± 0.28	0.90
Total cholesterol (mg/dl)			
t = 4 months	1,099 ± 291	1,220 ± 197	0.35
t = 5 months	1,158 ± 282	1,143 ± 126	0.91
t = 7 months	1,154 ± 230	1,278 ± 159	0.27
Triglycerides (mg/dl)*			
t = 4 months	147 ± 126	165 ± 168	0.87
t = 5 months	113 ± 95	102 ± 65	0.84
t = 7 months	172 ± 163	105 ± 17	0.52
Glucose (mg/dl)			
t = 4 months	152 ± 31	132 ± 25	0.29
t = 5 months	178 ± 40	156 ± 43	0.32
t = 7 months	180 ± 47	170 ± 47	0.67
Insulin (ng/dl)			
t = 4 months	0.52 ± 0.37	0.49 ± 0.45	0.91
t = 5 months	0.44 ± 0.39	0.32 ± 0.05	0.53
t = 7 months	0.23 ± 0.13	0.21 ± 0.06	0.79

Data for weight and fasting values for total cholesterol, triglycerides, glucose, and insulin are presented for the control and pioglitazone (PIO) groups in separate columns. Values of p between the control and PIO groups were determined with a Student *t* test and are shown in a separate column. Individual data except p values are represented as mean ± SD. *Indicated nonfasting.

average SUV_{max} of the corresponding animal. The AUC_{1min} and average SUV_{max} from corresponding animals were correlated. All correlations were measured using Pearson testing after normality of the data was established. All histologic data, animal characteristics data, and nonlinear regression imaging data were analyzed with a 2-tailed Student *t* test.

Power analysis. Retrospective power was computed using SAS Proc Mixed as previously described (23).

RESULTS

Study design, animal characteristics, and serum analysis. The study design is depicted in Figure 1. After 4 months of a high-cholesterol diet, significantly elevated total cholesterol levels were observed (Table 1). There were no significant baseline differences in total cholesterol between the control and pioglitazone-treated groups before treatment initiation (Table 1). There were no statistically significant differences in fasting serum glucose or insulin levels and in nonfasting triglycerides in either group throughout the study. Both groups had nearly identical weights throughout the study (Table 1). Fast protein liquid chromatography at baseline and after 3 months revealed no significant differences in lipoprotein profiles after pioglitazone treatment (Online Appendix Figure 1).

SUV correlates with tissue macrophage content and AUC correlates with neovascularization. We correlated the SUV_{max} and AUC_{1min} against macrophage density and neovessel counts, respectively, and found a strong positive correlation ($r^2 = 0.86$ and $p < 0.0001$, and $r^2 = 0.66$ and $p = 0.004$, respectively) (Figs. 2A and 2B), consistent with the results of previous studies (17,24). No strong correlation was found between SUV_{max} and neovessel count and between AUC_{1min} and macrophage density ($r^2 = 0.09$ and $p = 0.37$, and $r^2 = 0.19$ and $p = 0.18$, respectively) (Figs. 2C and 2D). The SUV_{max} and AUC_{1min} values did not correlate strongly ($r^2 = 0.17$, $p = 0.18$) (Fig. 2E).

Pioglitazone arrests inflammation progression as assessed by ^{18}F-FDG-PET/CT. On completion of baseline imaging, animals were divided into matched groups, 1 control group and 1 treatment group, with both groups displaying similar baseline SUV_{max} values (0.64 ± 0.05 and 0.62 ± 0.12, $p = 0.70$) (Figs. 3A and 3C and bar graph). The SUV versus time slope for the control group is positive, therefore indicating an increase in SUV_{max} ($p = 0.10$)

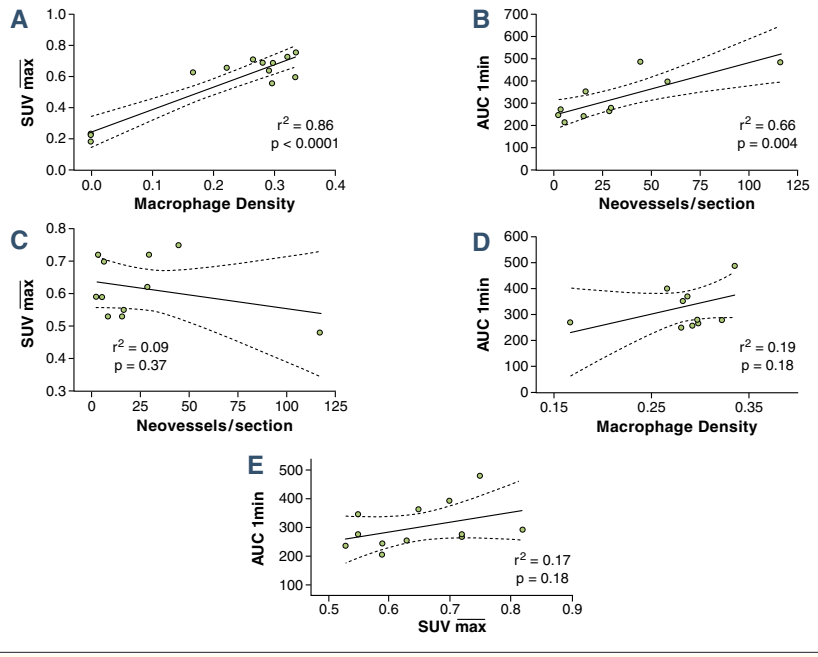

Figure 2. Regression Analysis

(A) Correlation between the maximum standard uptake value (SUV_{max}) generated from ^{18}F-fluorodeoxyglucose PET/CT imaging and macrophage density (stained area/intimal area) from histologic staining. **(B)** Correlation between mean area under the curve at 1 min (AUC_{1min}) generated from DCE-MRI imaging and neovessel count per histological section. **(C)** Correlation between SUV_{max} and neovessel count per histologic section. **(D)** Correlation between mean AUC_{1min} generated from DCE-MRI and macrophage density. **(E)** Correlation between SUV_{max} and mean AUC_{1min}. **Solid lines** = regression line; **dashed lines** = 95% confidence interval. Abbreviations as in Figure 1.

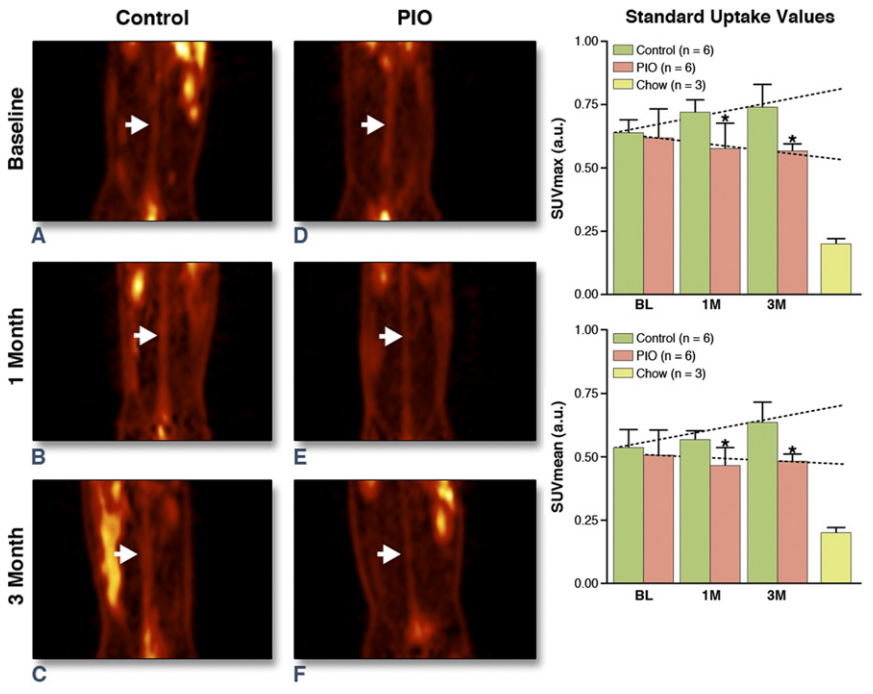

Figure 3. ^{18}**FDG-PET/CT**

(A to F) Coronal PET images through the abdominal aorta **(white arrowheads)** from 1 representative animal per group. **(A and D)** Baseline control and baseline pioglitazone (PIO) groups. **(B and E)** 1-month control and 1-month PIO groups. **(C and F)** Three-month control and PIO groups. On the **right,** 2 bar graphs summarize the changes in **(top)** SUV_{max} and **(bottom)** SUV mean at baseline (BL), 1 month (1M), and 3 months (3M) for both groups. Right-most bar shows values for nonatherosclerotic chow-fed animals. Values are represented as mean ± SD. *$p < 0.05$ when comparing control and PIO groups. Schematic slopes are indicated as **dashed lines**. a.u. = arbitrary units. Abbreviations as in Figures 1 and 2.

and SUV_{mean} ($p = 0.02$) over time. However, the SUV versus time slope for the treatment group was not statistically different from 0 (SUV_{max}: $p = 0.70$, SUV_{mean}: $p = 0.92$), indicating no significant progression in plaque inflammation. Comparison of the 2 slopes indicated a trend toward significance (SUV_{max}: $p = 0.15$, SUV_{mean}: $p = 0.1$). Comparison of SUV values between the 2 groups at 1 and 3 months showed significant differences ($p < 0.05$) for both SUV_{max} and SUV_{mean}. Nonatherosclerotic aged-matched animals on chow diet show minimal SUV values.

Pioglitazone decreases neovascularization as assessed by DCE-MRI. In analogy to the ^{18}F-FDG-PET/CT experiments, we applied DCE-MRI to assess inflammation and neovascularization in atherosclerotic plaques (Fig. 4). The AUC versus time slope for the control group was not statistically different from 0 for AUC measures (AUC_{1min}: $p = 0.33$, AUC_{2min}: $p = 0.18$). The AUC versus time slope for the treatment group was negative and significantly different from 0 for all AUC measures ($p < 0.01$). A trend toward significance was found when comparing the control and treatment groups slopes (AUC_{1min}: $p = 0.06$, AUC_{2min}: $p = 0.09$). There was a significant difference between baseline and 3-month AUC values in the treatment group (AUC_{1min}: $p = 0.01$).

Pioglitazone has no effect on vessel wall area as assessed by multicontrast-MRI. Multicontrast-MRI showed no significant changes in aortic wall area in either group during the study (Fig. 5).

Pioglitazone decreases plaque macrophages and oxidized phospholipids. Macrophage staining at the end of the imaging study revealed a significant decrease in macrophage density within the pioglitazone group compared with the control group (0.25 ± 0.05 arbitrary unit [AU] and 0.32 ± 0.02 AU, respectively, $p = 0.04$) (Figs. 6 and 7). A trend toward lower apolipoprotein B density was detected in the pioglitazone group compared with the control group (0.28 ± 0.03 AU and 0.34 ± 0.07 AU, respectively, $p = 0.12$) (Figs. 6 and 7). Pioglitazone treatment resulted in a 41% reduction in the oxidized phospholipid density compared with the control group (0.086 ± 0.026 AU and 0.146 ± 0.045 AU, respectively, $p = 0.03$) (Figs.

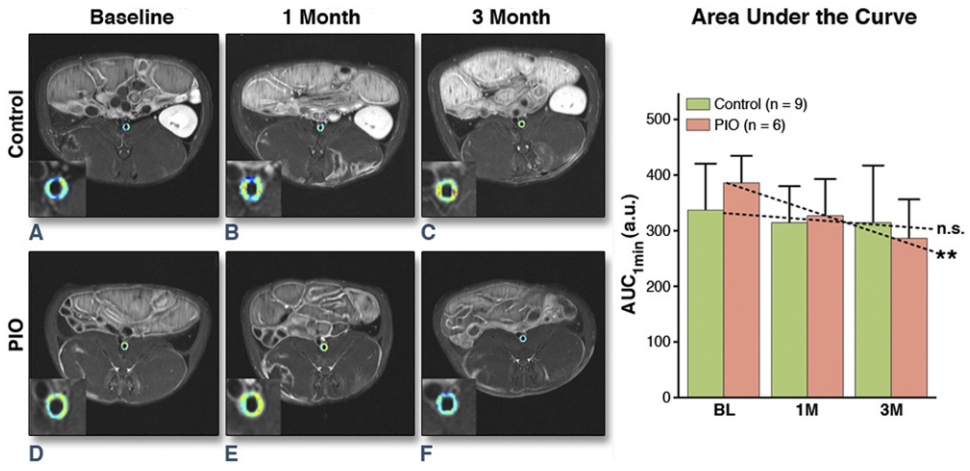

Figure 4. DCE-MRI

(A to F) Single-slice axial T1-weighted MRI scans with color-encoded overlay of the contrast signal at 1 min of the abdominal aorta with insert of the aorta. **(A and D)** Baseline control and baseline PIO groups. **(B and E)** One-month control and PIO groups. **(C and F)** Three-month control and PIO groups. Warm colors **(orange to red)** indicate higher AUC values and cold colors **(green to blue)** indicate lower AUC values. **Bar graph** summarizes the changes in the AUC at BL, 1M, and after 3M for the control and PIO groups. Values are represented as mean ± SD. *p < 0.05 when comparing baseline and 3M in the PIO group. **p = 0.01 when comparing individual slopes against 0. Schematic slopes are indicated as **dashed lines**. n.s. = nonsignificant. Abbreviations as in Figures 1, 2, and 3.

5 and 6). Average smooth muscle actin density was identical between groups (0.24 ± 0.075 AU and 0.24 ± 0.078 AU, respectively, p = 0.88) (Figs. 5 and 6). A trend toward lower neovessel content was observed in the pioglitazone-treated group (p = 0.12) (Fig. 6).

Power analysis of ^{18}F-FDG-PET/CT and DCE-MRI. ^{18}F-FDG-PET/CT determined SUV_{max} values had 30% power to detect a difference between individual group slopes, 43% power to detect a group effect, and 15% power to detect a time effect. The SUV_{mean} values had 40% power to detect a difference between individual group slopes, 37% power to detect a group effect, and 45% power to detect a time effect.

DCE-MRI determined AUC_{1min} values had 46% power to detect a difference between individual

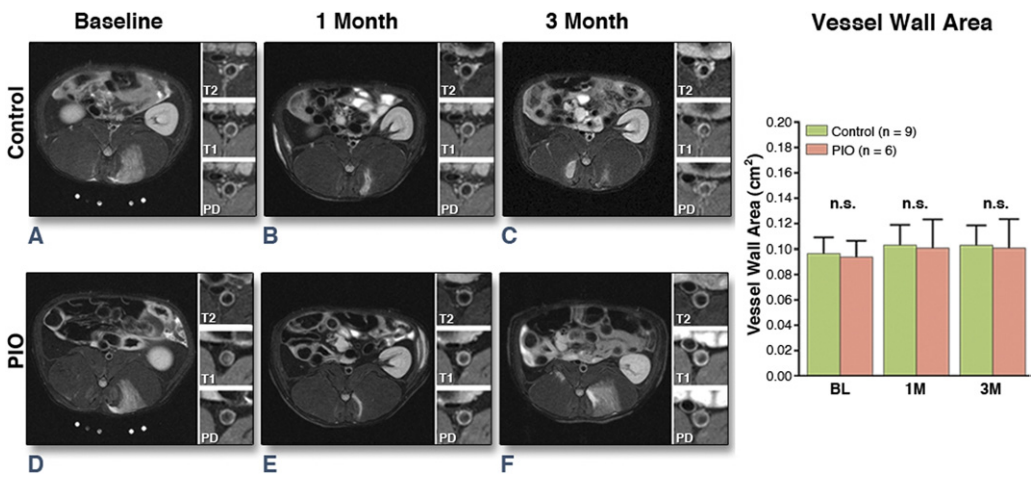

Figure 5. MC-MRI

(A to F) Single-slice axial T2-weighted representative MRI images with insert of the aorta with T2-weighting, T1-weighting, and proton density-weighting. **(A and D)** Baseline control and PIO groups. **(B and E)** One-month control and PIO groups. **(C and F)** Three-month control and PIO groups. **Bar graph** summarizes the changes in the vessel wall area at BL, 1M, and 3M of either the control or PIO group. Values are represented as mean ± SD. Abbreviations as in Figures 1, 3, and 4.

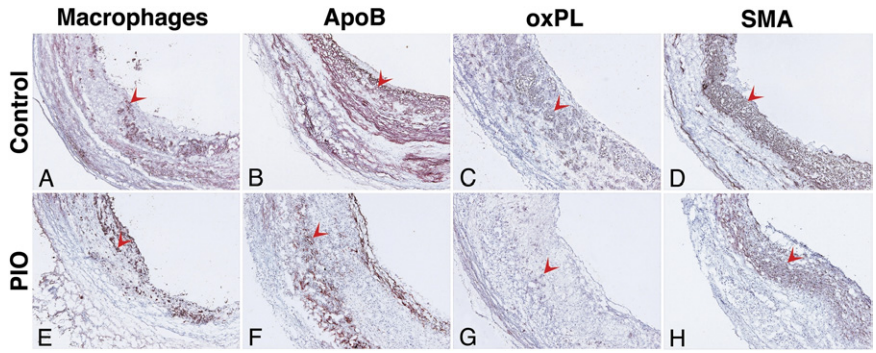

Figure 6. Immunohistologic Findings

Photomicrographs showing immunohistologic staining of the abdominal aorta after 3 months of **(A–D)** vehicle (control) and **(E–H)** PIO treatment. Staining **(red-brown, red arrowhead)** for **(A and E)** macrophages, **(B and F)** apolipoprotein B (ApoB), **(C and G)** oxidized phospholipids (OxPL), and **(D and H)** smooth muscle actin (SMA) is shown. Objective magnification: ×10. The lumen is on the right-hand side from the tissue. Abbreviation as in Figure 3.

group slopes, 14% power to detect a group effect, and 87% power to detect a time effect. The AUC_{2min} values had 39% power to detect a difference between individual group slopes, 15% power to detect a group effect, and 92% power to detect a time effect.

DISCUSSION

In this study, we showed significant modulation in inflammation in aortic plaques of atherosclerotic rabbits as measured noninvasively by ^{18}F-FDG-PET/CT and DCE-MRI on treatment with pioglitazone. The imaging results are confirmed by the histologic findings, which show a strong correlation of macrophage density and neovessel content with imaging parameters. In addition, this study provides insight to the diagnostic strengths of both FDG-PET and DCE-MRI while tracking antiatherosclerotic therapeutic intervention.

Previous studies have tested the potential of FDG-PET to track therapeutic intervention. Tahara et al. (25) investigated the effect of simvastatin on plaque inflammation by FDG-PET in the thoracic aorta of human subjects, whereas Ogawa et al. (26) investigated the effect of probucol on the aortic plaques of Watanabe heritable hyperlipidemic rabbits. In contrast with the work presented here, both of these studies showed no significant increase in FDG uptake in the control groups, whereas regression of inflammation was demonstrated by a significant decrease of FDG uptake over time in the treatment groups. This behavior is different from what we reported in our study, where we showed progression of inflammation in the control group and no change in FDG uptake over time in the treatment group. However, some significant differences between this study and the ones described above must be noted. For example, the dietary differences (dietary restrictions for patients and chow diet for rabbits as opposed to hyperlipidemic diet in this study with or without drug, depending on the group) and the different rabbit model used (Watanabe heritable hyperlipidemic rabbits versus New Zealand white rabbits). The only study in the literature investigating the use of DCE-MRI to track therapeutic intervention in atherosclerosis shows results comparable with those presented here, although

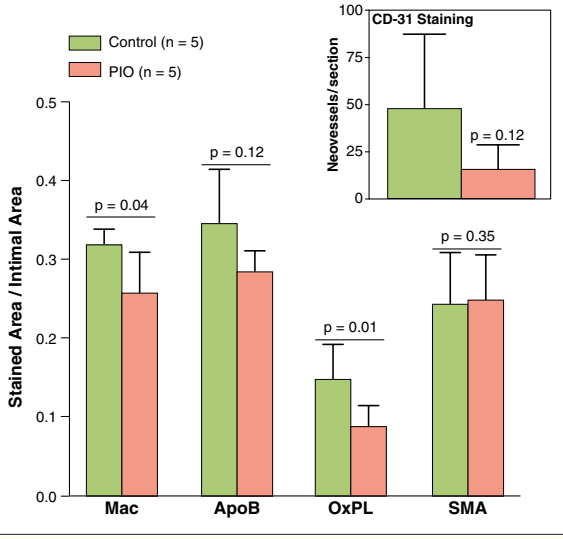

Figure 7. Summary of Immunohistologic Findings

Bar graph showing macrophages (Mac), ApoB, OxPL, and SMA staining at 3 months in vehicle and PIO-treated animals. **Insert** shows CD-31 staining for neovessels. Values are represented as mean ± SD. Individual p values between control and PIO groups indicated above bar graph. Abbreviations as in Figures 3 and 6.

the time frame of the 2 studies is considerably different (48 h vs. 3 months of treatment) (27).

In addition to showing the ability of FDG-PET and DCE-MRI to track therapeutic intervention with pioglitazone, this study sheds light on the possible complementary role in future clinical applications of the 2 methods. For example, FDG-PET showed an increase in plaque inflammation in the control group over time, whereas DCE-MRI measures did not change. Given the established correlation between FDG-PET and DCE-MRI with macrophages and neovessels, respectively, this may reflect a difference in the change of these histologic variables over time during plaque progression and may provide insight to the natural progression of aortic atherosclerosis in this specific rabbit model. More natural progression studies are needed to clarify this behavior and to plan future pre-clinical drug trials. The difference in FDG-PET and DCE-MRI measures in the treatment groups (impaired progression vs. regression) may reflect either the different sensitivity of the techniques or a different impact of pioglitazone on the related histologic variables (macrophages and neovessels, respectively). In this last case, the relationship between the 2 imaging techniques may be different for every new drug study planned with other therapeutic interventions.

CONCLUSIONS

In summary, we demonstrated the effectiveness of the PPARγ-agonist pioglitazone in promoting modulation of vascular inflammation in a rabbit model of atherosclerosis as evaluated by noninvasive imaging techniques and validated by histologic analysis. The ^{18}F-FDG-PET/CT and DCE-MRI analyses were used in this case as surrogate imaging markers of vascular inflammation. Both techniques already are available clinically, which stresses the translational aspect of this study. Dedicated prospective outcome studies are underway (HRP Initiative scheduled report in 2011 [28]) that will clarify the role of plaque inflammation imaging in patient risk stratification. Furthermore, novel antiatherosclerotic therapies are being developed and their role in clinical practice will need to be established. In this sense, the imaging tools described herein may become potent armaments for improved drug development and their translation into clinical practice. Dedicated future clinical studies in nondiabetic patient populations will be needed to evaluate pioglitazone's effect in atherosclerotic disease.

Acknowledgments

The authors thank Ash Rafique, RT(N) CNMT, BS, and Suzanna Zata, CNMT, for their support with the PET acquisitions.

Reprint requests and correspondence: Dr. Zahi A. Fayad, Translational and Molecular Imaging Institute, Mount Sinai School of Medicine, One Gustave L. Levy Place, Box 1234, New York, New York 10029. *E-mail: zahi.fayad@mssm.edu.*

REFERENCES

1. Dahlöf B. Cardiovascular disease risk factors: epidemiology and risk assessment. Am J Cardiol 2010;105:3A–9A.
2. Libby P, Ridker PM, Hansson GK. Inflammation in atherosclerosis: from pathophysiology to practice. J Am Coll Cardiol 2009;54:2129–38.
3. Ross R. Atherosclerosis—an inflammatory disease. N Engl J Med 1999;340:115–26.
4. Fuster V, Moreno PR, Fayad ZA, Corti R, Badimon JJ. Atherothrombosis and high-risk plaque: part I. Evolving concepts. J Am Coll Cardiol 2005;46:937–54.
5. Natarajan P, Ray KK, Cannon CP. High-density lipoprotein and coronary heart disease: current and future therapies. J Am Coll Cardiol 2010;55:1283–99.
6. deGoma EM, deGoma RL, Rader DJ. Beyond high-density lipoprotein cholesterol levels: evaluating high-density lipoprotein function as influenced by novel therapeutic approaches. J Am Coll Cardiol 2008;51:2199–211.
7. Marx N, Mach F, Sauty A, et al. Peroxisome proliferator-activated receptor-γ activators inhibit IFN-γ-induced expression of the T cell-active CXC chemokines IP-10, Mig, and I-TAC in human endothelial cells. J Immunol 2000;164:6503–8.
8. Takata Y, Kitami Y, Yang Z-H, Nakamura M, Okura T, Hiwada K. Vascular inflammation is negatively autoregulated by interaction between CCAAT/enhancer-binding protein-δ and peroxisome proliferator-activated receptor-γ. Circ Res 2002;91:427–33.
9. Collins AR, Meehan WP, Kintscher U, et al. Troglitazone inhibits formation of early atherosclerotic lesions in diabetic and nondiabetic low density lipoprotein receptor-deficient mice. Arterioscler Thromb Vasc Biol 2001;21:365–71.
10. Li AC, Brown KK, Silvestre MJ, Willson TM, Palinski W, Glass CK. Peroxisome proliferator-activated receptor gamma ligands inhibit development of atherosclerosis in LDL receptor-deficient mice. J Clin Invest 2000;106:523–31.
11. Nissen SE, Wolski K. Rosiglitazone revisited: an updated meta-analysis of risk for myocardial infarction and cardiovascular mortality. Arch Intern Med;170:1191–201.
12. Dormandy JA, Charbonnel B, Eckland DJA, et al. Secondary prevention of macrovascular events in patients with type 2 diabetes in the PROactive Study (PROspective pioglitAzone Clinical Trial In macroVascular Events): a randomised controlled trial. Lancet 2005;366:1279–89.

13. Rudd JH, Hyafil F, Fayad ZA. Inflammation imaging in atherosclerosis. Arterioscler Thromb Vasc Biol 2009;29:1009–16.
14. Chang K, Francis SA, Aikawa E, et al. Pioglitazone suppresses inflammation in vivo in murine carotid atherosclerosis: novel detection by dual-target fluorescence molecular imaging. Arterioscler Thromb Vasc Biol 2010; 30:1933–9.
15. Tawakol A, Migrino RQ, Bashian GG, et al. In vivo ^{18}F-fluorodeoxyglucose positron emission tomography imaging provides a noninvasive measure of carotid plaque inflammation in patients. J Am Coll Cardiol 2006;48:1818–24.
16. Rudd JHF, Warburton EA, Fryer TD, et al. Imaging atherosclerotic plaque inflammation with [18F]-fluorodeoxyglucose positron emission tomography. Circulation 2002;105: 2708–11.
17. Calcagno C, Cornily JC, Hyafil F, et al. Detection of neovessels in atherosclerotic plaques of rabbits using dynamic contrast enhanced MRI and 18F-FDG PET. Arterioscler Thromb Vasc Biol 2008;28:1311–7.
18. Rudd JH, Myers KS, Bansilal S, et al. Relationships among regional arterial inflammation, calcification, risk factors, and biomarkers: a prospective fluorodeoxyglucose positron-emission tomography/computed tomography imaging study. Circ Cardiovasc Imaging 2009;2:107–15.
19. Hyafil F, Cornily JC, Rudd JH, Machac J, Feldman LJ, Fayad ZA. Quantification of inflammation within rabbit atherosclerotic plaques using the macrophage-specific CT contrast agent N1177: a comparison with ^{18}F-FDG PET/CT and histology. J Nucl Med 2009;50:959–65.
20. Joner M, Farb A, Cheng Q, et al. Pioglitazone inhibits in-stent restenosis in atherosclerotic rabbits by targeting transforming growth factor-{beta} and MCP-1. Arterioscler Thromb Vasc Biol 2007;27:182–9.
21. McVicar JP, Kunitake ST, Hamilton RL, Kane JP. Characteristics of human lipoproteins isolated by selected-affinity immunosorption of apolipoprotein A-I. Proc Natl Acad Sci U S A 1984;81:1356–60.
22. Littell Ramon C, Miliken GA, Stroup WW, Wolfinger RD. SAS System for Mixed Models. Cary, NC: SAS Institute Inc., 1996.
23. Stroup WW. Mixed model procedures to assess power, precision, and sample size in the design of experiments. Proc Biopharmaceutical Section Am Stat Assoc 1999;15–24.
24. Tawakol A, Migrino RQ, Hoffmann U, et al. Noninvasive in vivo measurement of vascular inflammation with F-18 fluorodeoxyglucose positron emission tomography. J Nucl Cardiol 2005;12:294–301.
25. Tahara N, Kai H, Ishibashi M, et al. Simvastatin attenuates plaque inflammation: evaluation by fluorodeoxyglucose positron emission tomography. J Am Coll Cardiol 2006; 48:1825–31.
26. Ogawa M, Magata Y, Kato T, et al. Application of ^{18}F-FDG PET for monitoring the therapeutic effect of antiinflammatory drugs on stabilization of vulnerable atherosclerotic plaques. J Nucl Med 2006;47: 1845–50.
27. Lobatto ME, Fayad ZA, Silvera S, et al. Multimodal clinical imaging to longitudinally assess a nanomedical anti-inflammatory treatment in experimental atherosclerosis. Mol Pharm 2010;7:2020–9.
28. HRP initiative. Available at: http://www.hrpinitiative.com. Accessed August 22, 2011.

Key Words: atherosclerosis ■ dynamic contrast-enhanced magnetic resonance imaging ■ ^{18}F-fluorodeoxyglucose positron emission tomography/computed tomography ■ inflammation ■ pioglitazone.

▶APPENDIX

For an expanded Methods section, please see the online version of this article.